

1 **Defining the clonal dynamics leading to mouse skin tumour initiation**

2

3

4 Adriana Sánchez-Danés^{1,*}, Edouard Hannezo^{2,3,4,*}, Jean-Christophe Larsimont¹,
5 Mélanie Liagre¹, Khalil Kass Youssef¹, Benjamin D Simons^{2,3,4, #} and Cédric
6 Blanpain^{1,5, #}

7

8 ¹ Université Libre de Bruxelles, IRIBHM, Brussels B-1070, Belgium.

9 ² Cavendish Laboratory, Department of Physics, J. J. Thomson Avenue, Cambridge
10 CB3 0HE, UK.

11 ³ The Wellcome Trust/Cancer Research UK Gurdon Institute, University of Cambridge,
12 Tennis Court Road, Cambridge CB2 1QN, UK.

13 ⁴ Wellcome Trust-Medical Research Council Stem Cell Institute, University of
14 Cambridge, UK.

15 ⁵ WELBIO, Université Libre de Bruxelles, Brussels B-1070, Belgium.

16 * denotes co-first authors

17 # Corresponding authors

18

19

20 The changes that occur in cell dynamics following oncogenic mutation that lead to
21 the development of tumours are currently unknown. Here, using skin epidermis as
22 a model, we assessed the impact of oncogenic hedgehog signalling in distinct cell
23 populations and their capacity to induce basal cell carcinoma, the most frequent
24 cancer in humans. We found that only stem cells, and not progenitors, were
25 competent to initiate tumour formation upon oncogenic hedgehog signalling.
26 Interestingly, this difference was due to the hierarchical organization of tumour
27 growth in oncogene-targeted stem cells, characterized by an increase of symmetric
28 self-renewing divisions and a higher p53-dependent resistance to apoptosis, leading
29 to rapid clonal expansion and progression into invasive tumours. Our work reveals
30 that the capacity of oncogene-targeted cells to induce tumour formation is not only
31 dependent on their long-term survival and expansion, but also on the specific
32 clonal dynamics of the cancer cell of origin.

33

34

35 **Introduction**

36 Cancer arises through the acquisition of oncogenic mutations¹. How such
37 oncogenic mutations impact on the rate of stem and progenitor cell proliferation and the
38 proportion of divisions that result in symmetric and asymmetric fate is currently poorly
39 understood. Recent studies following oncogenic activation in mouse gut prior to tumour
40 formation showed that intestinal stem cells (SCs) acquire a proliferative advantage over
41 their wildtype neighbours, leading to precocious clonal fixation of mutant crypts^{2,3}.
42 However, the question of whether and how mutant crypts expand and progress into
43 invasive tumours remains unknown.

44

45 Basal cell carcinoma (BCC) is the most frequent tumour in humans with more
46 than 5 million new cases diagnosed each year worldwide. BCCs arise from the
47 constitutive activation of the hedgehog (HH) pathway through either Patched (Ptch) loss
48 of function or Smoothened (Smo) gain of function⁴. Different mouse models of BCC
49 using Ptch1 deletion or oncogenic SmoM2 mutant expression induce the formation of
50 tumours that resemble superficial human BCC⁵. The skin epidermis contains distinct
51 types of SCs that contribute to the homeostasis of discrete regions of epidermis⁶.
52 Interfollicular epidermis (IFE) is maintained by SCs targeted by K14-CreER and
53 committed progenitors (CPs) targeted by Inv-CreER in tail, ear, back and ventral skin
54 epidermis^{7,8}. Activation of oncogenic HH signalling through SmoM2 expression or
55 Patched1 deletion in these different tissues using K14-CreER, which targets both SCs
56 and CPs, induce BCC formation^{7,9-12}. However, the question of whether and how
57 SmoM2 expression in SCs and/or CPs drives BCC formation remains unresolved.

58

59

60 **Results**

61 **SCs but not CPs initiate BCC formation**

62 To determine whether SCs and CPs are both competent to induce BCC, we induced
63 oncogenic SmoM2 expression exclusively in CPs using Inv-CreER, and in both CPs
64 and SCs using K14-CreER⁷ at the same clonal density (Fig.1a and Extended Data
65 Fig.1a). As previously reported, activation of SmoM2 expression using K14-CreER
66 induced BCC, characterized by invasion into the dermis and branched morphology, in
67 both tail and ear epidermis (Fig. 1b)⁹⁻¹¹. In sharp contrast, activation of SmoM2
68 expression in CPs using Inv-CreER lead to preneoplastic lesions (including hyperplasia
69 and dysplasia) that did not progress into BCCs (Fig. 1b). These results suggest that only
70 IFE-SCs are competent to induce BCC following SmoM2-activation while IFE-CPs are
71 highly resistant.

72

73 We then assessed whether the competence of SCs and CPs to initiate BCC was
74 dependent on the oncogene or tumor suppressor gene used to activate HH signalling. To
75 this end, we induced Ptch1 deletion using K14- or Inv-CreER (Fig. 1c). Ptch1 deletion
76 using K14-CreER lead to BCCs arising from the IFE and the infundibulum (Fig. 1c). In
77 contrast, Ptch1 deletion using Inv-CreER, which targets some basal cells in the back and
78 ventral skin epidermis⁸, did not lead to the rapid development of BCC, and only rare
79 and small BCCs were observed 24w post-induction (Fig. 1c-d). These results reveal that
80 only IFE/infundibulum SCs are competent to induce BCC formation whereas CPs are
81 highly resistant, irrespective of the oncogene or tumour suppressor gene used to activate
82 HH signalling and body location (tail, ear, back and ventral skin).

83

84 Two distinct self-maintained compartments, scale and interscale, have been
85 described in tail epidermis¹³. To assess whether cells located in these two compartments
86 respond equally to oncogenic activation, we performed immunofluorescence using a
87 scale-specific marker (K31) and SmoM2-YFP on whole mount tail epidermis.
88 Interestingly, we found that BCCs arose from K14-CreER SmoM2 targeted cells
89 located only in the interscale (Fig. 1e). K14 clones in the interscale progressively lost
90 their normal differentiation program, as evidenced by the loss of spinous-like cells,
91 became hyperplastic, then dysplastic (Fig. 1f and Extended Data Fig. 1b-c). From 4 to 8
92 weeks (w) post-induction, around 15% of clones had progressed into BCC in interscale,
93 increasing to 40% after 24w (Fig. 1e-f). In contrast, K14 clones in scale never
94 progressed to BCC, and maintained a normal differentiation program for an extended
95 period, despite clonal expansion mediated by SmoM2 expression (Fig. 1e-f and
96 Extended Data Fig. 1b-c).

97

98 Together, these data indicate that the fate of oncogene targeted cells and the
99 ability of these cells to progress into BCC depends both on their location (scale versus
100 interscale) and cellular origin (SC versus CP). This prompted us to ask whether there
101 are regional differences in SC potential in tail epidermis even under homeostatic
102 conditions.

103 **Homeostasis of the interscale epidermis**

104 To gain quantitative insight into regional variation in SC potential, we performed
105 lineage tracing at homeostasis to determine whether scale and interscale are
106 differentially maintained. To this end, we compared the evolution of K14-CreER/Rosa-
107 YFP and Inv-CreER/Rosa-YFP targeted cells at single cell resolution over a 24w time-
108 course. Interestingly, although both broad, the distribution of clone sizes in the two

109 regions became increasingly divergent (Fig. 2a-b and Extended Data Fig. 2), confirming
110 the importance of regionalization in cellular dynamics (Supplementary Theory).

111

112 Consistent with our previous study⁷, the evolution of mean clone size of
113 progenitors targeted by Inv-CreER in the interscale fits well with the targeting of an
114 equipotent CP population presenting a small but statistically significant imbalance in
115 fate towards terminal differentiation (Fig. 2c-d). Similarly, the evolution of mean clone
116 size for K14-CreER cells is consistent with the targeting of a long-term self-renewing
117 SC population that divides more slowly than CPs (Fig. 2c-d). To define quantitatively
118 the dynamics of these two populations (cell cycle times, relative proportion of SCs and
119 CPs labelled by the K14-CreER and their fate probabilities), we made a joint fit to the
120 basal and suprabasal mean clone sizes, and extracted optimal parameters and confidence
121 intervals (Supplementary Theory).

122

123 To independently verify the predictions of the model, the persistence of Inv- and
124 K14-CreER targeted clones was used to infer the respective labelled cell fraction. As
125 expected from the labelling of a CP population, for Inv-CreER targeted clones, we
126 found that the labelled cell fraction decreased over time (Fig. 2e). In contrast, for K14-
127 CreER targeted clones, the labelled cell fraction increased over time, consistent with the
128 preferential targeting of the SC population (Fig. 2e). Strikingly, we obtained excellent
129 predictions for the labelled cell fraction for both K14- and Inv-CreER using parameters
130 extracted independently from a fit to the mean clone sizes (Fig. 2e). These results
131 provide compelling evidence in favour of a SC and CP hierarchy, and rule out the
132 possibility that the differences between K14- and Inv-CreER targeted clones are the
133 consequence of differential short-term “priming” of induced cells (Extended Data Fig.

134 3a). Importantly, the hierarchical model also predicted accurately the complete
135 distribution of clone sizes at all time points (Extended Data Fig. 3b-c) for both K14- and
136 Inv-CreER.

137

138 In sharp contrast, in the scale region of tail epidermis, both basal and suprabasal
139 clone size and persistence of K14- and Inv-CreER targeted cells were statistically
140 indistinguishable (Extended Data Fig. 4a and c). Crucially, the labelled cell fraction did
141 not change significantly between 2w and 24w post-labelling (Extended Data Fig.4c), an
142 indication that K14- and Inv-CreER mark the same balanced CP population¹³. We again
143 validated the model (Fig.4b) by showing that it could predict quantitatively both the
144 evolution of clonal persistence, as well the clone size distribution at all time points
145 (Extended Data Fig. 4b-d).

146

147 These results show that, during homeostasis, interscale is maintained by two
148 discrete populations; a comparatively slow-cycling SC and a more rapidly dividing CP
149 population, whereas scale is maintained by a single CP population. As well as unifying
150 diverging reports of maintenance hierarchy in tail epidermis^{7,13,14}, these findings raised
151 the question of whether the restriction of BCCs to the interscale correlated with the
152 regional localization of IFE SCs. To test this hypothesis, we assessed whether the same
153 regionalized lineage hierarchy persisted upon SmoM2 activation.

154

155 **Oncogene-targeted CPs are frozen into dysplasia**

156 To resolve the cellular dynamics underpinning to the differential sensitivity of SCs and
157 CPs to BCC initiation in interscale, we first studied the dynamics and proliferation
158 kinetics of Inv-CreER/Rosa-SmoM2 clones. Oncogenic activation in Inv-CreER CPs

159 lead to an increase of the average basal clone size, total clone size and clonal
160 persistence compared to homeostatic conditions (Fig. 3a-b and Extended Data Fig.5a-c),
161 as well as abnormal or decreased differentiation (Fig. 3a and Extended Data Fig. 1 b-c).
162 We assessed the average cell cycle time of SmoM2 Inv-CreER-targeted cells by first
163 marking proliferating cells using 24h of EdU administration, followed by variable
164 periods of continuous BrdU administration. From the co-labelling of EdU/BrdU, we
165 found that CPs divided on average every 3.6 ± 0.5 days at 4w following SmoM2
166 expression, 7.2 ± 0.6 days at 8w and 9.8 ± 0.3 days at 12w (Fig. 3c), indicating that the
167 average division rate of SmoM2 CPs decreases with time. Surprisingly, division rates
168 were uncorrelated with clone size at all time points, indicating that the decrease occurs
169 independently of clone size or stage of tumour progression (Extended Data Fig. 5d), and
170 consistent with the Inv-CreER oncogene targeted cells functioning as a single
171 equipotent population.

172

173 Since deregulation of apoptosis is also important for cancer formation¹, we
174 assessed whether apoptosis influences the clonal dynamics of oncogene targeted CPs. In
175 common with their normal counterpart, Inv-CreER targeted cells did not show evidence
176 of apoptosis over the first 6w following SmoM2 expression (data not shown). However,
177 from 8w on, about 60% of Inv-CreER targeted clones that presented hyperplasia or
178 dysplasia contained about 2-4% of apoptotic cells as measured by active caspase-3
179 immunostaining (Fig. 3d, Extended Data Fig. 5e-i).

180

181 Taking these rates (Fig. 3e) as an input, we could obtain an excellent fit to the
182 average clone size (Fig. 3f) with cell fate probabilities that remain constant over time
183 (symmetric renewal (PP): asymmetric division (PD): symmetric differentiation

184 (DD)=39%:45%:16%) (Fig. 3g). This result demonstrates that oncogenic expression in
185 CPs leads to enhanced clonal expansion and survival by promoting symmetric
186 proliferation over terminal differentiation. Such an imbalance would lead to exponential
187 clone growth if it were not counteracted by an ever-diminishing effective proliferation
188 rate, leading to a plateau in the mean basal clone size (Fig. 3f). Notably, the model
189 prediction provided a good fit to the clone size distribution at all time points (Fig. 3h).

190

191 Finally, to further verify the model, a low short-term dose of EdU was used to
192 mark a minority of dividing cells and their fate outcome was recorded 3 days later by
193 quantifying the basal and suprabasal localization of EdU doublets (Extended Data Fig.
194 5j). From these results, we could confirm a large imbalance between symmetric division
195 and terminal differentiation (35%).

196

197 Since the scale is maintained by a single progenitor pool, we wished to probe
198 whether its response to oncogenic activation was similar to interscale CPs. Crucially,
199 after an initial increase, the overall labelled cell fraction remained roughly constant over
200 time in scale between 8 and 24w, at a similar level for both K14- and Inv-CreER
201 (Extended Data Fig. 6a-c), suggesting that, in sharp contrast with interscale, both
202 populations behave identically upon oncogenic activation (Extended Data Fig. 6d).
203 Together, these results show that both interscale and scale CPs are resistant to BCC
204 formation upon oncogenic HH signalling, although interscale clones can persist longer
205 due to a larger fate imbalance and enhanced differentiation defects, while scale clones
206 rapidly converge towards balance. However, as human epidermis does not show scale
207 organization, the absence of BCC formation in the scale region might not have human
208 relevance.

209

210 **Oncogene-targeted SCs progress into BCC**

211 To gain insight into how SmoM2 expression in SCs promotes BCC formation, we then
212 performed a quantitative analysis of K14-CreER/Rosa-SmoM2 clones. Compared to
213 Inv-targeted clones, SmoM2 expression in K14-targeted cells lead to a more rapid and
214 persistent expansion of a fraction of clones (Fig. 4a-b and Extended Data Fig.7a-c) that
215 progressed into BCC, as well as the formation of smaller clones that did not show
216 tumour progression (Fig. 1e and 4b). This suggests that, in line with homeostatic
217 conditions, K14-CreER marks a fraction of tumour-like SCs, together with tumour-like
218 CPs, a heterogeneity that we verified using proliferation assays (Fig. 4c). Indeed, we
219 found that one population of K14-CreER targeted cells consisted of small clones that
220 displayed similar proliferation kinetics as Inv-CreER SmoM2 clones, while a second
221 population consisted of larger clones, which re-entered cell cycle significantly faster
222 (Fig. 4c, Extended Data Fig. 5d and 7d). The population of small K14-CreER targeted
223 clones (dysplasia and hyperplasia) also presented higher levels of apoptosis compared to
224 the larger clones (Fig. 4d and Extended Data Fig. 7e-i). As a result, even though the
225 proliferation of the larger clones also decreased with time (Fig. 4e and Extended Data
226 Fig.7j), their division rate was consistently higher than the Inv-CreER targeted
227 population (Fig. 4e).

228

229 To model BCC initiation, we adapted the hierarchical model obtained during
230 homeostasis and fitted jointly the mean basal and suprabasal clone sizes of all K14-
231 CreER-SmoM2 clones, taking as input the division rate as well as the fraction of SCs
232 initially labelled by the K14-CreER determined from measurements at homeostasis, and
233 used the fate choices of SCs as fitting parameters (Fig. 4f and Extended Data Fig. 7k).

234 In particular, we posited that SCs are imbalanced towards symmetric renewal, whereas
235 CPs derived from these cells remain slightly imbalanced toward symmetric
236 differentiation with the same fate probability as in homeostasis, which gave a good fit to
237 the average basal clone size (Fig. 4g). Notably, the measured clone size distributions
238 from 12w onwards could not be fit with a one-progenitor population model, in stark
239 contrast to the distributions of Inv-CreER-SmoM2 clones. Instead, the K14-CreER-
240 SmoM2 clone size distributions displayed a “double-exponential” decay, consistent
241 with the labelling of two distinct populations, as predicted quantitatively by the model
242 (Fig. 4h and Supplementary Theory). This shows that K14-CreER targets tumour-like
243 SCs making imbalanced stochastic fate choices, in addition to targeting the same
244 tumour-like CP population as Inv-CreER.

245

246 As a final consistency check, we addressed a key hallmark of the hierarchical
247 model, that SCs give rise to basal CPs in K14-CreER targeted clones. This predicts that
248 the fraction of cell divisions resulting in two basal cells should be greater in SC versus
249 CP-targeted clones. Indeed, short-term EdU pulse-chase experiments revealed that, in
250 BCC, most divisions (77%) lead to two basal cells (Extended Data Fig. 7l). In dysplasia,
251 the fraction of two EdU+ basal cell doublets was intermediate between the BCC and
252 Inv-CreER/Rosa-SmoM2 values (Extended Data Fig. 5j and 7l), consistent with a
253 mixture of SC and CP-targeted clones.

254

255 **p53 restricts CPs to progress into BCC**

256 Given the observed differences in apoptosis and division rates between oncogene
257 targeted SC and CP, we assessed whether p53, a tumour suppressor gene frequently
258 mutated in human BCC¹⁵ that controls cell cycle arrest and apoptosis¹⁶, was

259 differentially activated in SCs and CPs upon SmoM2 activation. Immunohistochemistry
260 revealed that p53 was more frequently found in SmoM2 clones arising from Inv-CreER
261 as compared to K14-CreER mice (Extended data Fig.8a). To determine whether p53
262 stabilization in oncogene targeted CPs restricts the potential of these progenitors to
263 generate BCC, we deleted p53 together with SmoM2 activation and assessed tumour
264 formation. Interestingly, p53 deletion in Inv-CreER targeted CPs leads to BCC in both
265 ear and tail epidermis (Fig. 5a). In the tail, BCCs were restricted to the interscale
266 whereas, in the scale, clones only progressed into dysplasia (Fig. 5b-c and Extended
267 Data Fig.8b). These results indicate that p53 restricts the competence of SmoM2
268 targeted CPs of the interscale to progress into BCC.

269

270 Although the proportion of clones that progress into BCC continued to be more
271 frequent and more rapid in K14-CreER targeted SCs, at 24w post-induction more than
272 half of interscale Inv-CreER targeted clones had progressed into BCC after p53 deletion
273 (Fig. 5c). The clonal persistence and clone size were increased upon p53 deletion in
274 both Inv-CreER/Rosa-SmoM2 and K14-CreER/Rosa-SmoM2 interscale clones,
275 although the clones were still bigger and more persistent in K14 targeted cells (Fig. 5b
276 and d and Extended Data Fig. 8c-e). These results indicate that, upon p53 deletion, both
277 oncogene targeted CPs and SCs present an increase in self-renewing divisions allowing
278 CPs to acquire the competence to form BCC upon SmoM2 expression.

279

280 We next determined whether the observed increase in clone size in the absence
281 of p53 in CPs and SCs was due to a decrease in apoptosis, an increase in proliferation or
282 both. Immunostaining for active caspase-3 8w after oncogenic activation showed that
283 large Inv-CreER/Rosa-SmoM2/p53fl/fl dysplastic and BCC clones displayed reduced

284 apoptosis, mirroring our observation in K14-CreER/Rosa-SmoM2 (Extended Data Fig.
285 8f). However, apoptosis was unchanged in Inv-CreER p53 deficient hyperplastic clones,
286 suggesting that p53 dependent and independent mechanisms control apoptosis in
287 oncogene-targeted cells (Fig. 5e and Extended Data Fig. 8g). EdU/BrdU double-pulse
288 experiments at 12w post-induction showed that deletion of p53 increased the rate of
289 proliferation in both Inv-CreER and K14-CreER oncogene targeted cells (Fig. 5f).
290 According to our model, this increase in the rate of division was sufficient, keeping all
291 other parameters constant, to explain the enhanced tumour growth (Fig. 5g). This
292 provides additional evidence that growth arrest in oncogene targeted CPs is a key
293 determinant in their inability to mediate BCC progression in the presence of p53.

294

295 In summary, our results demonstrate that p53 restricts the competence of CPs to initiate
296 BCC by promoting apoptosis and inducing cell cycle arrest in oncogene targeted CPs.

297

298 **Discussion**

299 In this study, we have defined the quantitative dynamics of BCC initiation at single cell
300 resolution, from the first oncogenic hit to the development of invasive tumours. These
301 results show that the proliferative hierarchical organization of skin epidermis is a key
302 determinant of tumour development, with only IFE SCs and not CPs competent to
303 initiate BCC following oncogenic HH signalling (Extended data Fig. 9). Even though
304 CP-derived clones survive and proliferate for months, they are surprisingly robust to
305 BCC transformation and invasion, becoming “frozen” in a pre-tumorigenic state. The
306 developmental cerebellar progenitors initiate medulloblastoma upon oncogenic HH
307 signaling^{17,18}, suggesting the developmental stage of progenitors may also dictate
308 competence for tumour initiation. The apparent long-term maintenance of some

309 oncogene targeted CPs stands in contrast to classical transient-amplifying cells in other
310 compartments, such as hair matrix in the skin or the non-Lgr5 crypt progenitors in gut,
311 which are resistant to tumour initiation because of their short lifespan¹⁹⁻²².

312

313 Our results show that IFE SCs reside solely in the interscale region, and have the
314 unique and regionalized competence to initiate large and invasive BCCs. Strikingly, this
315 regionalized hierarchical organization at homeostasis was maintained upon SmoM2
316 activation. Oncogene expression in SCs lead to a more rapid clonal expansion as
317 compared to CPs for two main reasons: the maintenance of hierarchical organization in
318 early pre-neoplastic lesions, leading to increased symmetric self-renewing divisions;
319 and the combined resistance to apoptosis and enhanced proliferation of SC-derived pre-
320 neoplastic lesions, leading to a larger effective growth rate. These two properties allow
321 SC-targeted tumours to escape the frozen-state that characterized CP-targeted pre-
322 neoplastic lesions, and thereby progress to an invasive phenotype.

323

324 Finally, our results show that p53 restricts the competence of CPs to undergo
325 BCC initiation by promoting apoptosis and inducing cell cycle arrest in oncogene
326 targeted CPs. Interestingly, although the division rates of CPs and SCs deficient for p53
327 are similar, SC-targeted tumours still grow to larger sizes than CP-targeted tumours,
328 suggesting that the hierarchical organization is at least partially maintained even after
329 two oncogenic hits. By establishing that sustained imbalance towards self-renewing
330 divisions and resistance to p53 mediated apoptosis and cell cycle arrest are the main
331 drivers of tumorigenesis, this study suggests that therapy promoting differentiation, p53
332 reactivation and apoptosis could present a promising avenue to promote BCC regression
333 and prevent tumour relapse.

334

335 **ACKNOWLEDGMENTS**

336 We would like to thank J-M. Vanderwinden and the LiMiF for the help with confocal
337 microscopy. C.B. is an investigator of WELBIO. A.S-D. and J.C.L. are supported by a
338 fellowship of the FNRS and FRIA respectively. B.D.S. and E.H. are supported by the
339 Wellcome Trust (grant number 098357/Z/12/Z and 110326/Z/15/Z). EH is supported by
340 a fellowship from Trinity College, Cambridge. This work was supported by the FNRS,
341 the IUAP program, the Fondation contre le Cancer, the ULB fondation, the foundation
342 Bettencourt Schueller, the foundation Baillet Latour, a consolidator grant of the
343 European Research Council.

344

345 **AUTHOR CONTRIBUTION**

346 A.S-D., C.B., E.H., B.D.S. designed the experiments, performed data analysis and wrote
347 the manuscript; A.S-D performed all of the biological experiments; E.H. performed all
348 the mathematical modelling. J.C.L and M.L. provided technical support. K.K.Y. made
349 initial observations pertinent to the study.

350

351 **AUTHOR INFORMATION**

352 Reprints and permissions information is available at www.nature.com/reprints. The
353 authors declare no competing financial interests. Readers are welcome to comment on
354 the online version of this article at www.nature.com/nature. Correspondence and
355 requests for materials should be addressed to C.B. (Cedric.Blanpain@ulb.ac.be) and
356 B.D.S (bds10@cam.ac.uk)

357

358 **REFERENCES**

359

- 360 1 Hanahan, D. & Weinberg, R. A. Hallmarks of cancer: the next generation. *Cell*
361 **144**, 646-674, doi:10.1016/j.cell.2011.02.013 (2011).
- 362 2 Vermeulen, L. *et al.* Defining stem cell dynamics in models of intestinal tumor
363 initiation. *Science* **342**, 995-998, doi:10.1126/science.1243148 (2013).
- 364 3 Snippert, H. J., Schepers, A. G., van Es, J. H., Simons, B. D. & Clevers, H.
365 Biased competition between Lgr5 intestinal stem cells driven by oncogenic
366 mutation induces clonal expansion. *EMBO Rep* **15**, 62-69,
367 doi:10.1002/embr.201337799 (2014).
- 368 4 Epstein, E. H. Basal cell carcinomas: attack of the hedgehog. *Nat Rev Cancer* **8**,
369 743-754 (2008).
- 370 5 Blanpain, C. & Simons, B. D. Unravelling stem cell dynamics by lineage
371 tracing. *Nat Rev Mol Cell Biol* **14**, 489-502, doi:10.1038/nrm3625 (2013).
- 372 6 Blanpain, C. & Fuchs, E. Stem cell plasticity. Plasticity of epithelial stem cells
373 in tissue regeneration. *Science* **344**, 1242281, doi:10.1126/science.1242281
374 (2014).
- 375 7 Mascré, G. *et al.* Distinct contribution of stem and progenitor cells to epidermal
376 maintenance. *Nature* **489**, 257-262, doi:10.1038/nature11393 (2012).
- 377 8 Lapouge, G. *et al.* Identifying the cellular origin of squamous skin tumors.
378 *Proceedings of the National Academy of Sciences of the United States of*
379 *America* **108**, 7431-7436, doi:10.1073/pnas.1012720108 (2011).
- 380 9 Youssef, K. K. *et al.* Identification of the cell lineage at the origin of basal cell
381 carcinoma. *Nat Cell Biol* **12**, 299-305, doi:10.1038/ncb2031 (2010).
- 382 10 Youssef, K. K. *et al.* Adult interfollicular tumour-initiating cells are
383 reprogrammed into an embryonic hair follicle progenitor-like fate during basal
384 cell carcinoma initiation. *Nat Cell Biol* **14**, 1282-1294, doi:10.1038/ncb2628
385 (2012).
- 386 11 Wong, S. Y. & Reiter, J. F. Wounding mobilizes hair follicle stem cells to form
387 tumors. *Proc Natl Acad Sci U S A* **108**, 4093-4098,
388 doi:10.1073/pnas.1013098108 (2011).
- 389 12 Kasper, M. *et al.* Wounding enhances epidermal tumorigenesis by recruiting hair
390 follicle keratinocytes. *Proc Natl Acad Sci U S A* **108**, 4099-4104,
391 doi:10.1073/pnas.1014489108 (2011).
- 392 13 Gomez, C. *et al.* The Interfollicular Epidermis of Adult Mouse Tail Comprises
393 Two Distinct Cell Lineages that Are Differentially Regulated by Wnt, Ederadd,
394 and Lrig1. *Stem cell reports* **1**, 19-27, doi:10.1016/j.stemcr.2013.04.001 (2013).
- 395 14 Clayton, E. *et al.* A single type of progenitor cell maintains normal epidermis.
396 *Nature* **446**, 185-189 (2007).
- 397 15 Bonilla, X. *et al.* Genomic analysis identifies new drivers and progression
398 pathways in skin basal cell carcinoma. *Nat Genet* **48**, 398-406,
399 doi:10.1038/ng.3525 (2016).
- 400 16 Chen, J. The Cell-Cycle Arrest and Apoptotic Functions of p53 in Tumor
401 Initiation and Progression. *Cold Spring Harbor perspectives in medicine* **6**,
402 doi:10.1101/cshperspect.a026104 (2016).
- 403 17 Schuller, U. *et al.* Acquisition of granule neuron precursor identity is a critical
404 determinant of progenitor cell competence to form Shh-induced
405 medulloblastoma. *Cancer Cell* **14**, 123-134 (2008).
- 406 18 Yang, Z. J. *et al.* Medulloblastoma can be initiated by deletion of Patched in
407 lineage-restricted progenitors or stem cells. *Cancer Cell* **14**, 135-145 (2008).
- 408 19 Barker, N. *et al.* Crypt stem cells as the cells-of-origin of intestinal cancer.
409 *Nature* **457**, 608-611 (2009).

410 20 White, A. C. *et al.* Defining the origins of Ras/p53-mediated squamous cell
411 carcinoma. *Proc Natl Acad Sci U S A* **108**, 7425-7430,
412 doi:10.1073/pnas.1012670108 (2011).
413 21 Lapouge, G. *et al.* Skin squamous cell carcinoma propagating cells increase with
414 tumour progression and invasiveness. *Embo J* **31**, 4563-4575,
415 doi:10.1038/emboj.2012.312 (2012).
416 22 Zhu, L. *et al.* Prominin 1 marks intestinal stem cells that are susceptible to
417 neoplastic transformation. *Nature* **457**, 603-607, doi:10.1038/nature07589
418 (2009).
419
420

421 **FIGURE LEGENDS**

422 **Figure 1. SCs but not CPs are competent to initiate BCC formation upon HH**
423 **activation**

424 (a) Genetic strategy to activate SmoM2 expression in SCs and CPs. (b) Immunostaining
425 of β 4-integrin/SmoM2 in ear and tail skin 24w after SmoM2 activation. (c)
426 Immunostaining of β 4-integrin/K14 in ventral skin 24w after Ptch1 deletion. (d)
427 Quantification of tumour burden (total tumour area divided by length of epidermis)
428 following Ptch1 deletion. Quantification of BCC number per length (mm) following
429 Ptch1 deletion. (n=4 Inv-CreER/Ptch1KO animals and n=3 K14CreER/Ptch1KO
430 animals (e) Immunostaining of K31/ SmoM2 in whole mount tail skin. (f)
431 Quantification of the morphology of SmoM2-expressing clones. Description of number
432 of counted clones is found in the method section. Hoechst nuclear staining in blue; scale
433 bars, 100 μ m. *P \leq 0,05, **P \leq 0,01, ***P \leq 0,001. Histograms and error bars represent the
434 mean and the standard error of the mean (s.e.m).

435

436

437 **Figure 2: Homeostatic renewal of mouse tail epidermis.**

438 (a, b) Distribution of basal clone sizes, in K14-CreER/Rosa-YFP (a) and Inv-
439 CreER/Rosa-YFP (b) epidermis. The number of clones analysed is indicated for each
440 time point and in the method section. (c) Mean basal (top) and suprabasal (bottom)
441 clone size in the interscale. The lines represent the model fit. (d) Cell fate probabilities
442 of SCs and CPs in the interscale, as extracted from the fits. (e) Clonal persistence (top)
443 and labelled cell fraction (bottom) in the interscale. Description of number of counted
444 clones is found in the method section. The lines are the predictions from the model
445 using only the parameters extracted in d. K14-CreER/Rosa-YFP clones display a net
446 expansion, whereas Inv-CreER/Rosa-YFP clones display a net contraction. Histograms

447 and error bars represent the mean and the s.e.m. Shaded areas represent 95% confidence
448 intervals for the model prediction (Supplementary Theory).

449

450

451 **Figure 3: SmoM2 expression in CPs induces clonal expansion that does not**
452 **progress into BCC.**

453 (a) Immunostaining for β -integrin, YFP and SmoM2 in Inv-CreER/Rosa-YFP and
454 Inv-CreER/Rosa-SmoM2 epidermis at different time points.(b) Distribution of Inv-
455 CreER/Rosa-YFP and Inv-CreER/Rosa-SmoM2 basal clone sizes. The number of
456 clones analysed in Inv-CreER/Rosa-SmoM2 is indicated for each time point and for
457 Inv-CreER/Rosa-YFP indicated in Fig. 2b. (c) Quantification of EdU/BrdU double-
458 labelled cells during continuous BrdU administration, at different time points post
459 clonal induction. The lines represent the model fit (Supplementary Theory). (d)
460 Quantification of the proportion of apoptotic cells in dysplastic, hyperplastic and
461 normally differentiating Inv-CreER/Rosa-SmoM2 clones 8w post-induction (n= 73
462 clones analysed from 4 independent experiments). (e) Division rate determined from
463 EdU/BrdU double-labelling experiments (data in black, fit in blue dashed line). (f)
464 Mean basal and suprabasal clone size in the interscale. The lines represent the model fit
465 from which we inferred the cell fate probabilities displayed in g. (g) Cell fate
466 probabilities of the tumour progenitor expressing SmoM2. (h) Basal clone size
467 distribution of Inv-CreER/Rosa-SmoM2 clones (black). Consistent with the hypothesis
468 of a single equipotent progenitor pool, all distributions are well-fit by single
469 exponential. Blue lines represent the model prediction using only the parameters
470 extracted from g. Shaded areas represent 95% confidence intervals for the model
471 prediction. D: dysplasia; H: hyperplasia; N: normal differentiation. Hoechst nuclear

472 staining in blue; scale bars, 10 μ m. Histograms and error bars represent the mean and the
473 s.e.m .

474

475

476 **Figure 4: SmoM2 expression in SCs induces tumour SCs that lead to BCC**
477 **formation.**

478 (a) Immunostaining for β -integrin, YFP and SmoM2 in K14-CreER/Rosa-YFP and
479 K14-CreER/Rosa-SmoM2 epidermis at different time points. (b) Distribution of K14-
480 CreER/Rosa-YFP and K14-CreER/Rosa-SmoM2 basal clone sizes. The number of
481 clones analysed for K14-CreER/Rosa-SmoM2 is indicated and for K14-CreER/Rosa-
482 YFP indicated in Fig. 2a. (c) Quantification of EdU/BrdU double-labelled cells
483 following continuous BrdU administration, at 8w post clonal induction for small K14-
484 CreER clones, Inv-CreER clones, and large K14-CreER clones. (d) Quantification of
485 the number of apoptotic cells in BCC, dysplastic, hyperplastic and normally
486 differentiating K14-CreER/Rosa-SmoM2 clones 8w post-induction (n= 117 clones
487 analysed from 4 independent experiments). (e) Division rate in large K14 clones
488 determined from double-labelling experiments (data in black, fit in red dashed line). (f)
489 Whisker plot of the mean basal clone size in the interscale. The boxes delineate the first
490 and third quartiles of the data, while the whiskers delineate the first and last decile of
491 the data. The thick continuous line is the best fit from the model from which we extract
492 the probability of fate choices in tumour SCs and progenitors displayed in g. The thin
493 dashed lines represent the predicted mean clone sizes of SCs- (top thin curve) and
494 progenitors- (bottom thin curve) derived clones alone. (g) Cell fate probabilities of the
495 tumour SC upon SmoM2 activation. (h) Basal clone size distribution of
496 K14CreER/SmoM2 clones (black). Red lines are the model prediction using only the

497 parameters extracted from g. Shaded areas represent 95% confidence intervals for the
498 model prediction. BCC: basal cell carcinoma; D: dysplasia; H: hyperplasia; N: normal
499 differentiation. Hoechst nuclear staining in blue; scale bars, 10 μ m. Histograms and error
500 bars represent the mean and the s.e.m..

501

502

503 **Figure 5: p53 deletion in CPs leads to BCC formation.**

504 (a) Immunostaining of β 4-integrin/SmoM2 in ear and tail skin of K14 and Inv-
505 CreER/Rosa-SmoM2/p53fl/fl mice 24w after Tamoxifen administration (b) Whole
506 mount immunostaining of K31/SmoM2 in tail epidermis overtime. (c) Quantification of
507 normal, hyperplastic, dysplastic and BCC clones in the interscale region. Description of
508 number of counted clones is found in the method section. (d) Distribution of basal clone
509 sizes in K14 and Inv-CreER/Rosa-SmoM2/p53fl/fl mice. The number of clones
510 analysed is indicated. Clone merger events were observed after 12w following
511 oncogenic activation in K14Cre-ER/Rosa-SmoM2/p53fl/fl preventing the accurate
512 quantification of clonal persistence and clone size at longer times. (e) Quantification of
513 the proportion of apoptotic cells in different clones (K14 n= 82 clones and Inv n=90
514 clones from 3 independent experiments). (f) Percentage of double-labelled EdU/BrdU
515 SmoM2-expressing cells after 6 days of continuous BrdU administration following a
516 24h pulse of EdU at 12w post-induction. *P \leq 0,05, **P \leq 0,01. (i) Mean basal clone size
517 in Inv-CreER/Rosa-SmoM2/p53fl/fl and K14-CreER/Rosa-SmoM2/p53fl/fl clones. The
518 prediction of the model is indicated by the blue and red lines. Histograms and error bars
519 represent the mean and s.e.m. Shaded areas represent 95% confidence intervals for the
520 model prediction in i. Scale bars, 100 μ m.

521

522 **METHODS**

523 **Mice**

524 K14CREER transgenic mice²³ were kindly provided by Elaine Fuchs, The Rockefeller
525 University; INVCREER were generated in our laboratory⁸. Ptch1 flox/flox mice²⁴ and
526 Rosa–SmoM2–YFP mice²⁵ were obtained from the JAX repository. p53fl/fl²⁶ mice
527 were obtained from the National Cancer Institute at Frederick.

528 Mouse colonies were maintained in a certified animal facility in accordance with
529 European guidelines. Experiments involving mice presented in this work were approved
530 by Comité d’Ethique du Bien Être Animal (Université Libre de Bruxelles) under
531 protocol number 483N, that states that animals should be euthanized if they present
532 tumours that exceed 1cm in diameter. The BCCs observed in this study were
533 microscopic and ranged from 1.5 mm to 100µm in diameter and in none of the
534 experiments performed, the tumours exceeded the limit described in protocol 483N.
535 Female and male animals have been used for all experiments and equal animal gender
536 ratios have been respected in the majority of the analysis, analysis of the different
537 mutant mice was not blind and sample size was calculated to reach statistical
538 significance.

539

540 **Skin tumour induction and clonal YFP expression**

541 For clonal induction 3-months-old mice were used. K14CreER/Rosa-YFP,
542 K14CreER/Rosa-SmoM2, K14CreER/SmoM2/p53fl/fl and K14CreER-Ptch1fl/fl mice
543 received an intraperitoneal injection of 0,1mg of Tamoxifen and Inv-CreER/Rosa-YFP,
544 Inv-CreER/Rosa-SmoM2, Inv-CreER/Rosa-SmoM2/p53fl/fl and INVCreER-Ptch1fl/fl
545 received a intraperitoneal injection of 2.5mg of Tamoxifen to achieve similar level of
546 recombination in the different models (Extended Data Figure 1a). Mice were sacrificed
547 and analysed at different time points following Tamoxifen administration.

548

549 **Immunostaining in sections**

550 The tail, ventral skin and ear skin were embedded in optimal cutting temperature
551 compound (OCT, Sakura) and cut into 5–8µm frozen sections using a CM3050S Leica
552 cryostat (Leica Microsystems).

553 Immunostainings were performed on frozen sections. Owing to the fusion of SmoM2
554 with YFP, SmoM2-expressing cells were detected using anti-GFP antibody. Frozen
555 sections were dried and then fixed with 4% paraformaldehyde/PBS (PFA) for 10min at

556 room temperature and blocked with blocking buffer for 1h (PBS, horse serum 5%, BSA
557 1%, Triton 0.1%). Skin sections were incubated with primary antibodies diluted in
558 blocking buffer overnight at 4 ° C, washed with PBS for 3 × 5 min, and then incubated
559 with Hoechst solution and secondary antibodies diluted in blocking buffer for 1h at
560 room temperature. Finally, sections were washed with PBS for 3 × 5 min at room
561 temperature and mounted in DAKO mounting medium supplemented with 2,5% Dabco
562 (Sigma). Primary antibodies used were the following: anti- GFP (Rabbit, 1/1000, BD,
563 ref. A11122), anti-K14 (Chicken, 1/4000, Covance, ref. PCK-153P-0100) and anti-B4-
564 integrin(Rat, 1:200, BD, ref.553745). The following secondary antibodies were used:
565 anti-rabbit, anti-rat, anti-chicken, conjugated to AlexaFluor488 (Molecular Probes) and
566 to rhodamine Red-X (JacksonImmunoResearch). Images of the immunostainings in
567 sections were acquired using an Axio Imager M1 microscope, an AxioCamMR3 camera
568 and the Axiovision software (Carl Zeiss).

569

570 **Immunostaining in whole mounts**

571 Whole mounts of tail epidermis were performed as previously described²⁷ and used to
572 quantify the proportion of surviving clones (Extended Data Fig.2b) as well as the basal
573 suprabasal and total clone size. Specifically, pieces of tail were incubated for 1h 37⁰C
574 in EDTA 20mM in PBS in rocking plate, then using forceps the dermis and epidermis
575 were separated and the epidermis was fixed for 30 minutes in PFA 4% in agitation at
576 room temperature and washed 3 times with PBS.

577 For the immunostaining: tail skin pieces were blocked with blocking buffer for 3h
578 (PBS, horse serum 5%, Triton 0.8%) in a rocking plate at room temperature. After, the
579 skin pieces were incubated with primary antibodies diluted in blocking buffer overnight
580 at 4 ° C, the next day they were washed with PBS-Tween 0.2% for 3 × 10 min at room
581 temperature, and then incubated with the secondary antibodies diluted in blocking
582 buffer for 3h at room temperature, washed 2x10 min with PBS-Tween 0.2% and washed
583 for 10min in PBS. Finally, they were incubated in Hoechst diluted in PBS for 30
584 minutes at room temperature in the rocking plate, washed 3x10 min in PBS and
585 mounted in DAKO mounting medium supplemented with 2,5% Dabco (Sigma).
586 Primary antibodies used were the following: anti-GFP (Rabbit, 1/100, BD, ref.
587 A11122), anti-GFP (Goat, 1:800,Abcam, ref. Ab6673), anti-active-caspase3 (Rabbit,
588 1/600,R&D, ref. AF835), anti-β4-integrin(Rat, 1:200, BD, ref. 553745) and anti-K31
589 (Guinea Pig, 1:200, Progen, ref. GP-hHa1). The following secondary antibodies were

590 used: anti-rabbit, anti-rat, anti-chicken, anti-goat and anti-guinea pig, conjugated to
591 AlexaFluor488 (Molecular Probes), to rhodamine Red-X (JacksonImmunoResearch)
592 and to Cy5 (1:400, Jackson ImmunoResearch).

593

594 **Analysis of clone survival, size and apoptosis**

595 Quantification of the proportion of surviving clones, as well as, total and basal clone
596 size was determined by counting the number of SmoM2-YFP and YFP-positive cells in
597 each clone using whole-mount tail epidermis. The different clones were imaged using
598 Z-stacks using a confocal microscope LSM 780 (Carl Zeiss) and orthogonal views were
599 used to count the number of basal and total number of SmoM2-YFP or YFP-positive
600 cells in each clone, as well as, the number of active-caspase3 positive cells in each
601 clone. K31 staining was used to classify the clones according to their location in the
602 scale or interscale regions.

603

604 **Proliferation assays**

605 To measure the kinetics of cell proliferation, a 24h continuous pulse of EdU followed
606 with a continuous pulse of BrdU were performed. Specifically, mice received at t=0 an
607 intraperitoneal injection of EdU (1mg/ml) and 0.1mg/ml EdU was added to their
608 drinking water for 24h. The next days the mice received a daily intraperitoneal
609 injection of BrdU (10mg/ml) and 1mg/ml of BrdU was added to their drinking water
610 during the 8 days of the continuous BrdU pulse. Mice were sacrificed at different time
611 points and whole mount stainings for the tail were performed. The pieces of tail were
612 first stained for anti-GFP (following the protocol described in the previous section).
613 Secondly, EdU staining was performed following the manufacturer's instructions
614 (Invitrogen). The pieces of tail were then washed in PBS and fixed again in PAF 4% for
615 10 minutes. After they were washed in PBS, blocked for 3h in the blocking buffer and
616 incubated for 20 min in HCl 1 N at 37 °C, washed three times with PBS-Tween 0.2%
617 and incubated overnight with Alexa 647-coupled anti-BrdU antibody (mouse, 1:200,
618 BD). The next day the tail pieces were washed in PBS, incubated in Hoechst for 30
619 minutes at room temperature in the rocking plate, washed 3x10 min in PBS and
620 mounted in DAKO mounting medium supplemented with 2,5% Dabco (Sigma). To
621 quantify the number of cells that incorporated EdU and/or BrdU, Z-stacks were
622 acquired for each individual clone and orthogonal views used to count.

623

624 **Immunohistochemistry**

625

626 For p53 immunohistochemistry, 4- μ m paraffin sections were deparaffinized, rehydrated,
627 followed by antigen unmasking performed for 20 min at 98°C in citrate buffer (pH 6)
628 using the PT module. Endogenous peroxidase was blocked using 3% H₂O₂ (Merck) in
629 methanol for 10 min at room temperature. Endogenous avidin and biotin were blocked
630 using the Endogenous Blocking kit (Invitrogen) for 20 min at room temperature. In p53
631 staining, nonspecific antigen blocking was performed using M.O.M. Basic kit reagent.
632 Mouse anti-p53 antibody (clone 1C12; Cell Signaling) was incubated overnight at 4°C.
633 Anti-mouse biotinylated in M.O.M. Blocking kit, Standard ABC kit, and ImmPACT
634 DAB (Vector Laboratories) was used for the detection of HRP activity. Slides were then
635 dehydrated and mounted using SafeMount (Labonord).

636

637 **Supplemental statistics**

638 For the quantification of the clone morphology of SmoM2-expressing clones in the
639 scale and interscale regions (Fig.1f), we counted in K14-CreER/Rosa-SmoM2 mice,
640 128,109,76,195,168 and 142 clones in the interscale region ; 141,116,74,94,78 and 69
641 clones in the scale region from 3,4,4,6,4 and 5 independent experiments at 1,2,4,8,12
642 and 24 w respectively. In Inv-CreER/Rosa-SmoM2 mice, 104,78,42,127,160 and 344
643 clones were counted in the interscale region; 94,54,99,90,99 and 39 clones in the scale
644 region from 4,4,4,5,4, and 8 independent experiments at 1,2,4,8,12,24 w respectively.

645

646 For the analysis of the clone size of the K14-CreER/Rosa-YFP mice (Fig. 2a,c and
647 Extended Data Fig. 2), we counted clones (both in scale and interscale) from two
648 independent experiments at 1w and 2w, five independent experiments at 4w, three
649 independent experiments at 8w, two independent experiments at 12w and four
650 independent experiments at 24 w. For the analysis of the clone size of the Inv-
651 CreER/Rosa-YFP mice (Fig. 2b-c, Extended Data Fig. 2), we counted clones (both in
652 scale and interscale) from two independent experiments at 1w and 2w, five independent
653 experiments at 4w, three independent experiments at 8w, four independent experiments
654 at 12w and three independent experiments at 24 w (see Data Source) .

655

656 For the clonal persistence of the K14-CreER/Rosa-YFP mice (Fig. 2e and Extended
657 Data Fig.2), we counted 167,176,129,100,47,246 clones in interscale and

658 184,109,75,66,19,103 clones in scale from 4,5,5,5,2,4, independent experiments at
659 1,2,4,8,12,and 24 w respectively. For 24w, we counted several areas per mice as the
660 number of clones was reduced (see Data Source).

661 For the clonal persistence of the Inv-CreER/Rosa-YFP mice (Fig. 2e and Extended Data
662 Fig.2), we counted 138,95,25,31,76,54 clones in interscale and 12,17,7,8,20,10 clones
663 in scale from 2,4,2,3,4,and 3 independent experiments at 1,2,4,8,12 and 24 w
664 respectively. For 12 and 24w, we counted several areas per mice as the number of
665 clones was low (see Data Source)

666

667 For the analysis of the clone size of the Inv-CreER/Rosa-SmoM2 mice (Fig. 3b,f, h,
668 Extended Data Fig. 5-6), we counted clones (both in scale and interscale) from two
669 independent experiments at 1w and 2w, from 4 independent experiments at 4w, from 6
670 independent experiments at 8w, from 6 independent experiments at 12w and from 4
671 independent experiments at 24 w.

672 For the clonal persistence of the Inv-CreER/Rosa-SmoM2 mice (Extended Data Fig 5-
673 6), we counted 65,39,71,51,27,18 clones in interscale and 67,27,47,31,12 and 6 clones
674 in scale from 2,2,4,3,2 and 2 independent experiments at 1,2,4,8,12 and 24w
675 respectively.

676 For the analysis of the clone size of the K14-CreER/Rosa-SmoM2 mice (Fig. 4b,f, h,
677 Extended Data Fig 6- 7), we counted clones (both in scale and interscale) from 3
678 independent experiments at 1w, from 2 independent experiments at 2w, 4w, from 6
679 independent experiments at 8w, from 4 independent experiments at 12w and from 2
680 independent experiments at 24w.

681 For the clonal persistence of the K14-CreER/Rosa-SmoM2 mice (Extended Data Fig.6-
682 7), we counted 122,63,81,79,74 and 68 clones in interscale and 89,46,37,42,31 and 16
683 clones in scale from 4,3,4,4,4 and 4 independent experiments at 1,2,4,8,12 and 24w
684 respectively.

685

686

687 For the cell proliferation kinetics experiments in the Inv-CreER/Rosa-SmoM2 mice
688 (Fig. 3c, e): At 4w post-induction, we counted 33 clones from 3 independent
689 experiments for 2 days of continuous BrdU, 30 clones from 2 independent experiments
690 for 4 days of continuous BrdU, 33 clones from 2 independent experiments for 6 days of
691 continuous BrdU. At 8w post-induction, we counted 41 clones from n=3 mice for 2 day

692 of continuous BrdU, 16 clones from 2 independent experiments for 4 day of continuous
693 BrdU, 30 clones from 2 independent experiments for 6 day of continuous BrdU and 24
694 clones from 2 independent experiments for 8 day of continuous BrdU. At 12w post-
695 induction, we counted 19 clones from 2 independent experiments for 2 day of
696 continuous BrdU, 26 clones from 2 independent experiments for 4 day of continuous
697 BrdU, 27 clones from 2 independent experiments for 6 day of continuous BrdU and 31
698 clones from 2 independent experiments mice for 8 day of continuous BrdU. For the 2w
699 post-induction data point, we use solely continuous BrdU incorporation, and counted 54
700 clones from 2 independent experiments.

701 For the cell proliferation kinetics experiments in the K14-CreER/Rosa-SmoM2 mice
702 (Fig. 4c,e): At 4w post-induction, we counted 56 clones from 3 independent
703 experiments for 2 days of continuous BrdU, 39 clones from 3 independent experiments
704 for 4 days of continuous BrdU, 29 clones from 3 independent experiments for 6 days of
705 continuous BrdU. At 8w post-induction, we counted 30 clones from 2 independent
706 experiments for 2 days of continuous BrdU, 25 clones from 2 independent experiments
707 for 4 days of continuous BrdU, 63 clones from 3 independent experiments for 6 days of
708 continuous BrdU and 41 clones from 3 independent experiments for 8 days of
709 continuous BrdU. At 12w post-induction, we counted 20 clones from 2 independent
710 experiments for 2 days of continuous BrdU, 21 clones from 2 independent experiments
711 for 4 days of continuous BrdU, 28 clones from 2 independent experiments for 6 days of
712 continuous BrdU and 26 clones from 2 independent experiments for 8 days of
713 continuous BrdU.

714

715 For the quantification of the clone morphology in absence of p53 interscale (Fig.5c).
716 For K14-CreER/Rosa-SmoM2/p53fl/fl mice 186,217,90,343,452 and 543 clones from
717 3,3,2,3,5 and 5 independent experiments and for Inv-CreER/Rosa-SmoM2/p53fl/fl
718 95,98,199,271,263 and 210 clones from 3,3,3,4,4 and 4 independent experiments were
719 analysed at 1,2,4,8,12 and 24 w respectively. In the quantification in the scale region
720 (Extended Data Fig.8b) for K14-CreER/Rosa-SmoM2/p53fl/fl 178,204,100,132,232
721 and 120 clones were counted from 3,3,2,3,5, and 5 independent experiments 1,2,4,8,12
722 and 24 w respectively. For Inv-CreER/Rosa-SmoM2 82,127,167,136,62 and 153 clones
723 were counted from 2,3,3,4,4 and 5 independent experiments 1,2,4,8,12 and 24 w
724 respectively.

725

726

727 For the cell proliferation kinetics experiments in the Inv-CreER/Rosa-SmoM2/p53fl/fl
728 mice (Fig. 5f) at 12w post-induction 34 clones from 3 independent experiments were
729 counted. For the cell proliferation kinetics experiments in the K14-CreER/Rosa-
730 SmoM2/p53fl/fl mice (Fig. 5f) at 12w post-induction 44 clones from two independent
731 experiments were counted.

732

733 For the clonal persistence experiments in Inv-CreER/Rosa-SmoM2/p53fl/fl,
734 132,78,68,58 and 89 clones from 4,3,3,3 and 5 independent experiments were counted
735 at 1,2,4,8,12 and 24 w and in K14-CreER/Rosa-SmoM2/p53fl/fl mice 124,82,53,76 and
736 100 clones were counted from 4,3,2,3 and 4 independent experiments at 1,2,4,8 and
737 12w respectively (Extended Data Fig.8e). (See Data Source)

738

739

740

741 **References**

742

- 743 23 Vasioukhin, V., Degenstein, L., Wise, B. & Fuchs, E. The magical touch:
744 genome targeting in epidermal stem cells induced by tamoxifen application to
745 mouse skin. *Proc Natl Acad Sci U S A* **96**, 8551-8556 (1999).
- 746 24 Uhmman, A. *et al.* The Hedgehog receptor Patched controls lymphoid lineage
747 commitment. *Blood* **110**, 1814-1823, doi:10.1182/blood-2007-02-075648
748 (2007).
- 749 25 Mao, J. *et al.* A novel somatic mouse model to survey tumorigenic potential
750 applied to the Hedgehog pathway. *Cancer Res* **66**, 10171-10178 (2006).
- 751 26 Jonkers, J. *et al.* Synergistic tumor suppressor activity of BRCA2 and p53 in a
752 conditional mouse model for breast cancer. *Nat Genet* **29**, 418-425 (2001).
- 753 27 Braun, K. M. *et al.* Manipulation of stem cell proliferation and lineage
754 commitment: visualisation of label-retaining cells in wholemounts of mouse
755 epidermis. *Development* **130**, 5241-5255 (2003).

756

757

758

759

760

761

762

763 **Extended Data Figure legends**

764

765 **Extended data Figure 1. The fate of oncogene targeted clones is determined by the**

766 **initial targeted cell (SC or CP) and their location in scale or interscale regions**

767 (a) Orthogonal view used to quantify the number of clones, cells stained with β 4-
768 integrin/SmoM2. (left). Quantification of the number of clones induced 1 week after
769 Tamoxifen administration in scale and interscale regions in K14-CreER/Rosa-SmoM2
770 (n=4 animals, 0.1mg Tamoxifen) and Inv-CreER/ Rosa-SmoM2 (n=3 animals, 2.5 mg
771 Tamoxifen) (right). (b) Immunostaining for β 4-integrin and SmoM2 in K14-
772 CreER/Rosa-SmoM2 and Inv-CreER/Rosa-SmoM2 clones located in the scale and
773 interscale regions, 8w after oncogene activation. (c) Immunostaining for the
774 differentiation marker keratin-10, K10, and SmoM2 in K14-CreER/Rosa-SmoM2 and
775 Inv-CreER/Rosa-SmoM2 clones 8w after oncogene activation, showing absence of
776 differentiated cells in K14-CreER/Rosa-SmoM2 clones and alteration of the
777 differentiation in Inv-CreER/Rosa-SmoM2 clones. Hoechst nuclear staining is
778 represented in blue; Scale bars, 10 μ m.

779

780 **Extended data Figure 2. Evolution of K14-CreER/Rosa-YFP and Inv-**

781 **CreER/Rosa-YFP clones in scale and interscale regions**

782 (a) Whole mount immunostaining for YFP/K31 in K14-CreER/Rosa-YFP mice and Inv-
783 CreER/Rosa-YFP mice upon Tamoxifen administration. (b) Scheme representing the
784 area of tail epidermis (area comprised by 6 groups of triplets of hair follicles,
785 highlighted in black) that is used to quantify the clone number and persistence. (c)
786 Distribution of K14-CreER/Rosa-YFP and Inv-CreER/Rosa-YFP total clone sizes as
787 measured by total cell content of surviving clones, imaged by confocal microscopy on

788 whole-mount tail epidermis from 1 to 24 weeks following Tamoxifen administration.
789 The number of analyzed clones is indicated for each time point. Hoechst nuclear
790 staining is represented in blue; scale bars, 100 μ m. Histograms and error bars represent
791 the mean and the standard error of the mean (s.e.m)

792

793

794

795

796 **Extended data Figure 3. The interscale is maintained by two cell populations**
797 **during homeostasis.**

798 (a) Evolution in time of the total labelled cell fraction under three hypotheses. For a
799 perfect single population of equipotent balanced progenitors, the labelled cell fraction
800 remains constant. For a single population of equipotent balanced progenitors displaying
801 short-term priming, the labelled cell fraction increases transiently for the cells primed to
802 divide, and decreases transiently for the cells primed to differentiate, but after the
803 priming period, both fractions remain constant at different values. For two populations
804 organised in a hierarchy, the labelled fraction of the progenitors decreases continuously
805 to zero, while the labelled fraction of the stem cells continuous increases to reach a
806 steady state value, corresponding to its average progeny size. (b) Cumulative basal
807 clone size distribution of Inv-CreER/Rosa-YFP clones at homeostasis in the interscale
808 upon Tamoxifen administration. (c) Cumulative basal clone size distribution of K14-
809 CreER/Rosa-YFP clones at homeostasis in the interscale upon Tamoxifen
810 administration. Clonal distributions are plotted in log-plot, error bars indicate S.D.,
811 thick lines are the model prediction and shaded area indicate 95% confidence intervals
812 in the model prediction.

813

814

815

816

817 **Extended data Figure 4. The scale is maintained by a single population during**
818 **homeostasis.**

819 (a) Evolution of mean surviving basal (top) and suprabasal (bottom) clone size in the
820 scale for K14-CreER/Rosa-YFP (red) and Inv-CreER/Rosa-YFP (blue). In contrast to
821 the interscale, in the scale K14- and Inv-CreER clones behave identically, indicative of
822 a single progenitor pool. The lines are the fit from the model from which we extract the
823 fate choices of progenitors displayed in b. (b) Fate choices of the equipotent progenitor
824 pool in the scale, as extracted from the fits. (c) Clonal persistence (top) and labelled cell
825 fraction (bottom) in the scale for K14-CreER/Rosa-YFP (red) and Inv-CreER/Rosa-
826 YFP (blue). The blue and red lines are the predictions of the model (see Supplementary
827 Notes for details) using only the parameters extracted in b. K14- and Inv-CreER clones
828 behave similarly and display near-perfect long-term balance. For the clonal persistence
829 data, we examined in each mouse a randomly chosen area shown in Extended data Fig.
830 2b. Error bars represent the s.e.m. (d) Cumulative basal clone size distribution of K14-
831 CreER/Rosa-YFP clones at homeostasis in the scale upon Tamoxifen administration.
832 One should note that there were too few Involucrin clones in the scale to plot
833 meaningful distributions. Clonal distributions are plotted in log-plot, error bars indicate
834 S.D, thick lines are the model prediction and shaded area indicate 95% confidence
835 intervals in the model prediction.

836

837 **Extended data Figure 5. Clonal dynamics of interscale InvSmoM2 clones is**

838 **consistent with a single imbalanced population of progenitors slowing down in**
839 **time**

840 (a) Distribution of Inv-CreER/Rosa-YFP (black) and Inv-CreER/Rosa-SmoM2 (red)
841 clone sizes as measured by total cell content, imaged by confocal microscopy on whole
842 mount tail epidermis from 1w to 24w following Tamoxifen administration. The number
843 of clones analysed in Inv-CreER/Rosa-SmoM2 is indicated in Fig 3b. The number of
844 clones counted in Inv-CreER/Rosa-YFP is as indicated in Fig. 2b. (b) Evolution of the
845 clonal persistence for interscale Inv-CreER/Rosa-SmoM2 clones. (c) Labelled cell
846 fraction for interscale Inv-CreER/Rosa-SmoM2 clones. (d) Fraction of EdU/BrdU
847 double-labelled cells as a function of basal clone size at 8w for Inv-CreER/Rosa-
848 SmoM2 clones, for 2 (left), 4 (centre) and 6 (right) days of continuous BrdU
849 incorporation. (e) Immunostaining for β 4-integrin, SmoM2 and active-caspase-3 in Inv-
850 CreER/Rosa-SmoM2 clones at 8w post-induction. (f) Percentage of dysplastic,
851 hyperplastic and normally differentiating Inv-CreER/Rosa-SmoM2 clones presenting at
852 least one active-caspase positive cell within the clone at 8w post-induction (n= 73
853 clones analysed from 4 independent experiments). (g) Quantification of the number (%)
854 of basal and suprabasal apoptotic cells in dysplastic, hyperplastic and normally
855 differentiating Inv-CreER/Rosa-SmoM2 clones 8w after SmoM2-activation. (h)
856 Percentage of dysplastic, hyperplastic and normally differentiating Inv-CreER/Rosa-
857 SmoM2 clones presenting apoptosis in basal and suprabasal compartments 8w after
858 oncogenic activation. (i) Cumulative distribution of the fraction of basal apoptosis as a
859 function of basal cell number in an Inv-CreER/Rosa-SmoM2 clone at 8w (data in blue).
860 The green line is the expected theoretical distribution of apoptotic fraction if apoptosis
861 occurred randomly (following a Poisson process), in any clone with the same
862 probability. The data is statistically different from the random theory, showing that

863 apoptosis clusters in certain clones at a given time point. (j) Short-term fate outcome of
864 progenitors in Inv-CreER/Rosa-SmoM2 clones at 8w, as assessed by using EdU as a
865 clonal marker. We count only cell doublets and classify them as either basal-basal,
866 basal-suprabasal, or suprabasal-suprabasal. (n=47 clones from 3 independent
867 experiments). Immunostaining for β 4-integrin, EdU and SmoM2 showing the different
868 type of cell fate outcomes found in Inv-CreER/Rosa-SmoM2 clones. D: dysplasia; H:
869 hyperplasia; N: normal differentiation. Hoechst nuclear staining is represented in blue;
870 Scale bars, 10 μ m. Histograms and error bars represent the mean and the s.e.m.

871

872 **Extended data Figure 6. Clonal dynamics of Inv-CreER/Rosa-SmoM2 and K14-**
873 **CreER/Rosa-SmoM2 clones in the scale are similar**

874 (a) Evolution of mean surviving basal clone sizes (top) and labelled cell fraction
875 (bottom), for K14-CreER/Rosa-SmoM2, in the scale. (b) Evolution of mean surviving
876 basal clone sizes (top) and labelled cell fraction (bottom), for Inv-CreER/Rosa-SmoM2,
877 in the scale. Whereas the interscale clones show net expansion, scale clones, both Inv-
878 CreER and K14-CreER, show near balance at the population level. (c) Evolution of the
879 persistence of K14-CreER/Rosa-SmoM2 (green) and Inv-CreER/Rosa-SmoM2 (purple)
880 clones in the scale. Strikingly, and in contrast to the interscale, both K14 and Involucrin
881 clones have the same persistence. (d) Mean basal clone size, normalised by the mean
882 clone size at 1w for both Inv-CreER and K14-CreER clones. Even though one can see
883 on panel (a) and (b) that the final clone size is higher in K14, this is fully explained by
884 short-term differences in fate during the first week indicative of short-term priming for
885 K14. Correspondingly, the evolution of the labelling fraction is very similar for K14
886 and Involucrin in scale. Therefore, K14-CreER/Rosa-SmoM2 and Inv-CreER/Rosa-
887 SmoM2 in scale display the same long-term kinetics upon oncogenic activation,

888 consistent with the one-population model uncovered at homeostasis. Error bars
889 represent the s.e.m.

890

891 **Extended data Figure 7. Clonal dynamics of interscale K14-CreER/Rosa-SmoM2**
892 **clones is consistent with two populations**

893 (a) Distribution of K14-CreER/Rosa-YFP (black) and K14-CreER/Rosa-SmoM2 (red)
894 clone sizes as measured by total cell content, imaged by confocal microscopy on whole
895 mount tail epidermis from 1w to 24w post-induction. The number of clones analyzed
896 for K14-CreER/Rosa-SmoM2 is indicated in Fig 4b; the number of clones counted in
897 K14-CreER/Rosa-YFP is as indicated in Fig. 2a. (b) Evolution of the clonal persistence
898 and (c) labelled cell fraction for K14-CreER/Rosa-SmoM2 clones in the interscale. (d)
899 Fraction of EdU/BrdU double-labelled cells as a function of basal clone size at 8w for
900 K14-CreER/Rosa-SmoM2 clones, for 2 (left), 4 (centre) and 6 (right) days of
901 continuous BrdU incorporation. (e) Immunostaining for β 4-integrin, SmoM2 and
902 active-caspase-3 in K14-CreER/Rosa-SmoM2 clones 8w after SmoM2 activation. (f)
903 Percentage of BCC, dysplastic, hyperplastic and normally differentiating clones
904 presenting at least one active-caspase-3 positive cell at 8w post-induction (n=117 clones
905 analysed from 4 independent experiments). (g) Quantification of the number (%) of
906 basal and suprabasal apoptotic cells in dysplastic, hyperplastic and normally
907 differentiating Inv-CreER/Rosa-SmoM2 clones 8w after SmoM2-activation. (h)
908 Percentage of dysplastic, hyperplastic and normally differentiating Inv-CreER/Rosa-
909 SmoM2 clones presenting basal and suprabasal apoptosis 8w after oncogenic activation.
910 (i) Cumulative distribution of the fraction of basal apoptosis as a function of basal cell
911 number in a K14-CreER/Rosa-SmoM2 clone at 8w (data in red). The green line is the
912 expected theoretical distribution of apoptotic fraction if apoptosis occurred randomly

913 (following a Poisson process), in any clone with the same probability. The data is
914 statistically different from the random theory, showing that apoptosis clusters in certain
915 clones at a given time point. (j) Quantification of EdU/BrdU double-labelled cells as a
916 function of the period of continuous BrdU incorporation for large K14 clones at 4w
917 (black), 8w (orange) and 12w (red) post clonal induction. The dashed lines represent the
918 model fit (Supplementary Theory). (k) Whisker plot of the suprabasal clone size in the
919 interscale. The boxes delineate the first and third quartiles of the data, while the
920 whiskers delineate the first and last decile of the data at a given time point. The thick
921 continuous line is the best fit from the model from which we extract the probability of
922 fate choices in tumor SC and progenitors, displayed in Fig.4g. The thin lines represent
923 the mean clone sizes of stem cells (top curve) and progenitors (bottom curve) if they
924 were alone. (l) Short-term fate outcome of progenitors in K14-CreER/Rosa-SmoM2
925 clones at 8w, as assessed by using EdU as a clonal marker. We count only cell doublets
926 and classify them as either basal-basal, basal-suprabasal, or suprabasal-suprabasal.
927 (n=49 clones from 3 independent experiments) Immunostaining for β 4-integrin, EdU
928 and SmoM2 in K14-CreER/Rosa-SmoM2 hyperplastic/dysplastic clones (top) and in
929 BCC (bottom panel). BCC: basal cell carcinoma; D: dysplasia; H: hyperplasia; N:
930 normal differentiation; SB: suprabasal. Hoechst nuclear staining is represented in blue;
931 Scale bars, 10 μ m. Error bars represent the s.e.m.

932

933 **Extended data Figure 8. Effect of p53 deletion in the cellular dynamics of CPs and**
934 **SCs**

935 (a) IHC staining for p53 in Inv-CreER/Rosa-SmoM2 and K14-CreER/Rosa-SmoM2
936 clones 12 w post-induction (b) Quantification of normal, hyperplastic, dysplastic and
937 BCC clones in scale region of K14CreER/Rosa-SmoM2/p53fl/fl and Inv-CreER/Rosa-

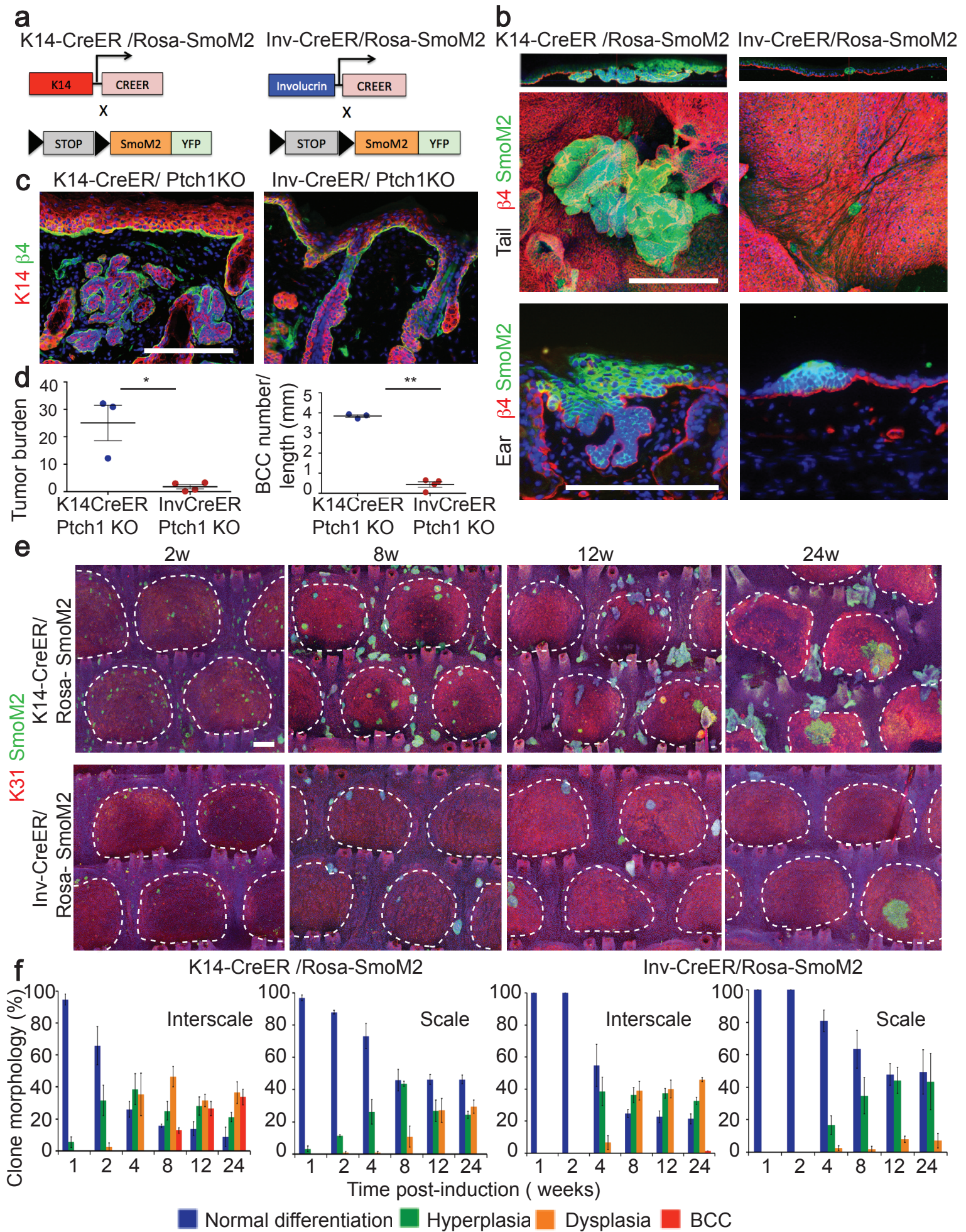
938 SmoM2/p53fl/fl mice. Description of number of counted clones is found in the method
939 section.(c) Distribution of clone sizes as measured by total cell content, imaged by
940 confocal microscopy on whole mount tail epidermis. The number of clones analysed is
941 indicated in Fig 5d. Clone merger events were observed after 12w following oncogenic
942 activation in K14Cre-ER/Rosa-SmoM2/p53fl/fl preventing the accurate quantification
943 of clonal persistence and clone size at long times. (d) Comparison of basal clone size
944 distribution of Inv-CreER/Rosa-SmoM2/p53fl/fl vs. Inv-CreER/Rosa-SmoM2 and K14-
945 CreER/Rosa-SmoM2/p53fl/fl vs. K14-CreER/Rosa-SmoM2 at 8w and 12w upon
946 Tamoxifen administration. (e) Evolution of the clonal persistence of Inv-CreER/Rosa-
947 SmoM2/p53fl/fl and K14-CreER/Rosa-SmoM2/p53fl/fl clones. (f) Immunostaining of
948 active-caspase-3 and SmoM2 8w post-induction in Inv-CreER/Rosa-SmoM2/p53fl/fl
949 (g) Quantification of the proportion of apoptotic clones in Inv-CreER/Rosa-
950 SmoM2/p53fl/fl (n=90 clones from 3 independent experiments), and K14-CreER/Rosa-
951 SmoM2/p53fl/fl (n=82 animals from 3 independent experiments) 8w post-induction.
952 Hoechst nuclear staining is represented in blue; Scale bars, 10µm. Error bars represent
953 the s.e.m.

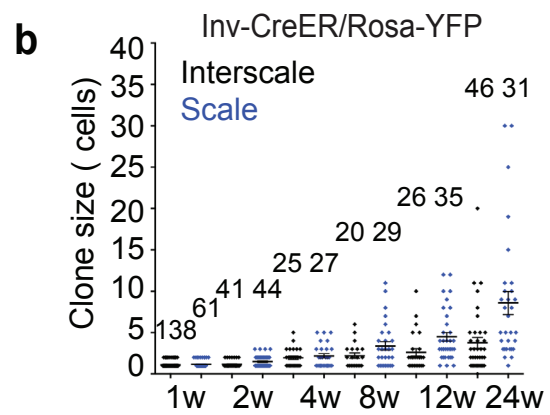
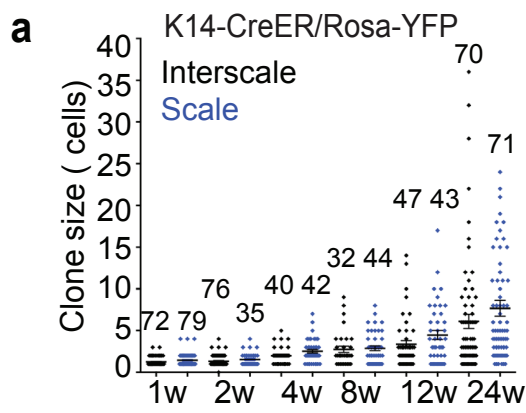
954

955 **Extended data Figure 9. Model of BCC initiation**

956 Activation of SmoM2 in SCs leads to the generation of BCC due to an increase in cell
957 proliferation and resistance to apoptosis. However, activation of p53 in SmoM2-
958 expressing CPs restricts the progression of dysplastic clones to BCC by promoting
959 apoptosis and cell cycle arrest. Deletion of p53 in CPs allows them to progress into
960 BCC.

961





Interscale: K14-CreER/Rosa-YFP and Inv-CreER/Rosa-YFP

